TRENDS IN SCIENCES 2025; 22(10): 10462
https://doi.org/10.48048/tis.2025.10462 RESEARCH ARTICLE

Synthesis of $AgMn_3O_4$/C and AgSn/C Cathodes and Pd/C Anode Catalyst for Sorbitol Membraneless Alkaline Fuel Cells

Pintira Chayboonchoo[1], Supansa Dampat[1], Sonchai Intachai[1], Bancha Yingngam[3] and Chakkrapong Chaiburi[2,*]

[1]Department of Physical Sciences, Faculty of Science and Digital Innovation, Thaksin University, Phatthalung Campus, Phatthalung 93210, Thailand
[2]Faculty of Engineering, Thaksin University, Phatthalung Campus, Phatthalung 93210, Thailand
[3]Faculty of Pharmaceutical Sciences, Ubon Ratchathani University, Ubon Ratchathani 34190, Thailand

([*]Corresponding author's e-mail: chakkrapong@tsu.ac.th)

Received: 24 April 2025, Revised: 15 June 2025, Accepted: 6 July 2025, Published: 30 July 2025

Abstract

This study explored the synthesis of catalysts for sorbitol membraneless alkaline fuel cells (SMAFC) that target both cathode and anode fuels. The synthesized catalysts included $AgMn_3O_4$/C, AgSn/C, and Pd/C for the cathode and anode. This research examined the electrochemical properties of alkaline fuel oxidation by employing sorbitol as the fuel. Various sorbitol concentration ratios, ranging from 0.1 to 0.5 M per 0.1 M alkaline KOH solution, were analyzed using cyclic voltammetry with a scan rate of 0.01 V/s. At a concentration of 0.1 M sorbitol, the Pd/C catalyst was identified as an anode catalyst. The oxidation sites exhibited the greatest potential difference within the range of –0.5 to 0.5 V, resulting in a maximum current density of 0.75 mA/cm^{-2}. The $AgMn_3O_4$/C and AgSn/C catalysts were tested as cathode side catalysts in the reduction reaction using sorbitol solution concentrations ranging from 0.1 to 0.5 M per 0.1 M alkaline KOH solution. The reduction reaction of the catalyst decreased with increasing sorbitol concentration. It appears that hydrocarbon adsorption did not result in any oxidation reactions. As sorbitol fuel crosses from the anode to the cathode side, the cathode catalyst must be resistant to oxidation reactions. An alkaline membraneless sorbitol fuel cell was tested, achieving peak performance with specific catalyst pairings. The cell, fueled by a 0.1 M sorbitol solution and 0.1 M potassium hydroxide at the anode (2.5 mL/min flow) and air at the cathode (3 mL/min flow), generated a maximum current density of 0.40 A/m^2 and a maximum power density of 0.155 W/m^2. These results were observed using a Pd/C catalyst for the anode and an AgSn/C catalyst for the cathode. The average calculated value of the number of electrons involved in the catalytic reaction (n) was 3.20.

Keywords: Alkaline membraneless fuel cell, Catalyst, Sorbitol, Anode, Cathode, Fuel cell, Oxidation reaction, Reduction reaction

Introduction

Energy has an indispensable role in human life, serving as the foundation for transportation, communication, and education, while also driving the advancement of industrial economies [1]. As global energy demand is projected to surge by 50% between 2001 and 2025, significant increases in consumption are anticipated across residential, agricultural, industrial, and transportation sectors [2]. Broadly defined as the capacity to perform work or cause movement through the application of force, energy exists in various forms and is typically classified into consumable (non-renewable) energy - such as fossil fuels, which are depleted with use - and renewable energy sources, including solar, hydro, wind, and geothermal power. The escalating global population further intensifies pressure on finite energy reserves, stressing the urgent

need to ensure adequate energy supplies. Thus, expanding and optimizing the use of renewable energy sources has become essential for addressing future energy shortages and promoting sustainable development.

Nevertheless, given the impending depletion of conventional natural energy sources, achieving sustainable energy systems necessitates advances in science, technology, and innovation to develop practical and efficient forms of renewable energy. Among these, fuel cells, particularly those utilizing chemical energy, have emerged as a promising technology that converts the chemical energy of fuels such as hydrogen, methane, methanol, natural gas, and coal gas directly into electrical energy through electrochemical processes, thereby providing an alternative to finite energy sources without relying on combustion [3]. Direct alcohol fuel cells are among the most widely adopted fuel cell technologies, with alkaline fuel cells noted for their high efficiency, use of cost-effective and environmentally benign catalysts, and low rates of corrosion. The oxidation of methanol or formate is more efficient in alkaline media compared to acidic environments, particularly when Pd-based anode catalysts are alloyed with metals like Au, Ni, Cu, or Co. Methanol, ethanol, and polyalcohols are the most common fuels employed in these systems [4]. The adoption of fuel cell technology results in reduced air pollution and has wide-ranging applications, including in transportation (e.g., hydrogen-powered vehicles) and the development of long-life backup batteries [5]. Alkaline fuel cells are available in diverse designs, with material selection tailored to the specific type of cell and operating environment. For instance, the structural and chemical characteristics of materials - such as anion exchange membranes and electrodes with high electrocatalytic activity - are critical for optimizing performance. Alkaline fuel cells offer high electrical efficiency, dynamic operational suitability, and compact design [6]. However, they present both advantages and challenges compared to traditional and newer fuel cell technologies, with ongoing research focusing on the advancement of catalysts, especially for oxygen reduction and hydrogen oxidation reactions, to enhance overall cell efficiency and durability [7].

Building on these considerations, the present study investigates the application of sorbitol solutions in fuel cells. As a member of the widely used polyalcohol group, sorbitol offers promising oxidation efficiency, likely due to its favorable electron transfer characteristics [8]. While most existing research has focused on glucose-based fuel cells, studies specifically examining sorbitol in membraneless alkaline fuel cells remain scarce. Nonetheless, research on glucose fuel cells, given the structural similarity between glucose and sorbitol, provides a relevant foundation for exploring the potential of sorbitol in fuel cell applications.

Catalyst materials for the oxygen reduction reaction (ORR)

Kruusenberg *et al.* [9] performed a detailed analysis of non-platinum catalyst materials for fuel cell applications, evaluating them within membrane-electrode assemblies (MEAs) incorporating a Tokuyama membrane and benchmarking them against commercial noble metals. Their work concentrated on Co and Fe phthalocyanine catalysts supported by multi-walled carbon nanotubes (MWCNTs). Assessments of the oxygen reduction reaction (ORR) kinetics in 0.1M KOH solution via rotating disk electrodes showed that Co phthalocyanine-based electrodes consistently yielded higher current densities than those employing Fe phthalocyanine. Weiss *et al.* [10] explore recent developments concerning the stability and durability of Fe-N-C electrocatalysts for the oxygen reduction reaction (ORR) in operational environments. Their review identifies active site de-metallization and carbon corrosion as key factors leading to swift initial performance degradation, stressing the involvement of H_2O_2 radicals in these processes. Beyond discussing the current state of Fe-N-C electrocatalysts, the authors put forth several specific recommendations for improving these materials to achieve competitive stability and sustainability. To advance fuel cell technology, Xu *et al.* [11] sought efficient, durable, and affordable electrocatalysts for the slow oxygen reduction reaction (ORR). They developed dual metal single-atom catalysts (SACs), specifically Zn/Co-N-C, featuring unique $Co\text{-}N_4$ and $Zn\text{-}N_4$ local structures. These catalysts showed excellent ORR performance, boasting a half-wave potential ($E_{1/2}$) of 0.938 V (vs. RHE) and impressive stability, with only an 8.5 mV drop in $E_{1/2}$ after 50,000 cycles. Moreover, they achieved a record-setting peak power density of about 1 $W \cdot cm^{-2}$ in actual

alkaline fuel cell operation, making them a new benchmark among reported SACs.

Catalyst materials for the oxygen reduction reaction (ORR) of glucose alkaline fuel cell

Ho *et al.* [12] demonstrated the successful synthesis of $CoMn_2O_4$/nitrogen-doped carbon (NC) nanocomposites using a straightforward ionothermal method, targeting their application in direct glucose alkaline fuel cells (DGAFCs). The incorporation of an ionic liquid enabled the formation of a nitrogen-doped carbon-supported $CoMn_2O_4$ spinel, which served as a highly efficient electrocatalyst for the oxygen reduction reaction (ORR). This novel nanocomposite exhibited electrocatalytic performance nearly equivalent to that of commercial Pt/C catalysts, with a half-wave potential of 0.81 V and a peak diffusion-limiting current density of 5.2 $mA \cdot cm^{-2}$. When employed as an air cathode in a direct glucose fuel cell (DGFC), the $CoMn_2O_4$/NC composite facilitated a peak power density of 23.72 $W \cdot m^{-2}$, underscoring its practical potential. Relatedly, Hu *et al.* [13] investigated glucose fuel cells (GFCs) employing abiotic catalysts for sustainable energy generation in portable and wearable devices. They developed a cobalt oxide-integrated carbon nanofiber (CoOx@CNF) catalyst, featuring mixed-valence cobalt oxides, by partially oxidizing pyrolyzed electrospun cobalt and polyacrylonitrile fibers. By manipulating the oxidation conditions and cobalt precursor content, they were able to finely control the cobalt valence states within the catalyst. Electrocatalytic assessments revealed that the inclusion of CoO within the CoOx@CNF matrix substantially enhanced its performance by increasing the density of active sites for glucose electrooxidation. As a result, a GFC utilizing this CoOx@CNF anode (comprising both CoO and Co_3O_4) achieved a peak power density of 270 $\mu W \cdot cm^{-2}$, outperforming previously reported Co_3O_4-based GFCs and accentuating its promise for next-generation green energy devices.

Moreover, Dai *et al.* [14] introduced a simple one-step in-situ hydrothermal approach to synthesize reduced graphene oxide (rGO) nanocomposites co-doped with nitrogen, sulfur, and transition metals (Ni, Co, Fe), among which the rGO-NS-Ni catalyst demonstrated superior glucose oxidation performance. When employed as the anode catalyst in direct glucose alkaline fuel cells (DGAFCs), rGO-NS-Ni achieved an impressive current density of 148.0 $mA \cdot cm^{-2}$ and a peak power density of 48 $W \cdot m^{-2}$, indicating its strong electrocatalytic potential. In a parallel advancement, Suzuki *et al.* [15] developed a rapid and efficient method for fabricating glucose fuel cells by uniformly coating palladium onto nickel wire meshes, utilizing a mixture of palladium chloride solution and sodium dodecyl sulphate. The resulting fuel cell could be assembled in under 30 min within a plastic container by layering a glucose-potassium hydroxide solution, 2 palladium-coated nickel wire mesh electrodes, and a cellophane membrane, representing a significant reduction in production time compared to traditional techniques. Huang *et al.* [16] investigated the platinum-catalyzed oxidation of D-glucose in neutral electrolytes for use in implantable energy devices, revealing 2 primary reaction pathways - direct oxidation and oxidation via OH adsorption. Their solvothermal synthesis of PtPd and Pt_2Pd anode catalysts resulted in a notable maximum power density of 27.6 $\mu W \cdot cm^{-2}$ for the PtPd catalyst, advancing the development of glucose fuel cells with improved performance. Xu *et al.* [17] addressed the persistent challenge of glucose oxidation kinetics in abiotic glucose fuel cells by engineering a 3-dimensional nitrogen-doped porous carbon material (NCZIF-8) with an extensive surface area of 944 m^2/g, serving as a catalyst support. Through in-situ reduction, they dispersed platinum nanoparticles at a low 10 wt% loading onto NCZIF-8, yielding a catalyst (10% Pt/NCZIF-8) with uniformly distributed active sites and enhanced durability. This strategy markedly improved catalytic efficiency for glucose electrooxidation, which illustrates the importance of material innovation in advancing fuel cell technologies.

Furthermore, the porous structure of NCZIF-8 improved glucose transport, while the embedded Pt NPs mitigated the negative impact of oxygen on the oxidation reaction. The durability of the 10% Pt/NCZIF-8-modified anode was confirmed by a minimal 7.83% reduction in peak current density after 300 cyclic voltammetry (CV) cycles. Basu *et al.* [18] investigated direct glucose fuel cells (DGFCs) as a potential power source for low-power portable devices. Their research focused on understanding why these fuel cells lose efficiency, specifically by studying the electro-oxidation of both glucose and fructose on a PtRu/C catalyst in an

alkaline environment using cyclic voltammetry. They built a basic DGFC with a PtRu/C anode and an activated coal cathode to examine how different concentrations and temperatures of glucose and KOH affected performance. They found that with a 0.3 M glucose solution in 1M KOH, the open circuit voltage (OCV) reached 0.91V, and this voltage increased with higher glucose concentrations. The peak power density was highest at 1.38 $mW.cm^{-2}$ using 0.2M glucose in 1M KOH at 30°C, but it decreased when glucose concentration or temperature rose further. To understand the role of fructose in performance decline, they tested the cell with 0.2 M fructose in 1 M KOH, which yielded a lower peak power density of 0.57 $mW.cm^{-2}$. The DGFC ran continuously for 260 h under a steady 500Ω load, eventually settling at a voltage of 0.21 V. Liu's work [19] highlights the significant potential of glucose fuel cells (GFCs) as a sustainable energy solution. This promise stems from glucose's renewable, readily available, affordable, abundant, non-toxic, and easily storable nature - qualities that make it an attractive energy source. Despite these benefits, ongoing efforts are needed to boost GFC performance. Liu's aim is to combine a literature review with a technological discussion on GFCs and their membranes using bibliometric analysis. The goal is to spark new ideas and help researchers overcome existing challenges in developing high-performance GFCs.

Catalyst materials for the oxygen reduction reaction (ORR) of sorbitol alkaline fuel cell

Daşdelen *et al.* [20] systematically evaluated the effectiveness of various support materials - fumed silica (FS), reduced graphene oxide (rGO), and an FS-rGO hybrid - for gold nanoparticle (Au) anode catalysts in sorbitol fuel cells. Their findings revealed that the Au@FS-rGO catalyst exhibited superior current density for sorbitol oxidation, with FS demonstrating a greater ability than rGO to enhance both catalytic activity and long-term stability. In a related development, Askari *et al.* [21] engineered a ternary nanocatalyst composed of nickel cobalt oxide ($NiCo_2O_4$), reduced graphene oxide, and platinum (Pt), specifically tailored for sorbitol oxidation in fuel cell applications. Comparative analyses with catalysts containing only individual or binary combinations of these materials showed that the $NiCo_2O_4$–rGO/Pt catalyst achieved the highest current density (57.2 $mA \cdot cm^{-2}$ at 10 $mV \cdot s^{-1}$), the lowest onset potential (0.64 V), and superior stability under repeated use. Torres-Pacheco *et al.* [22] further contributed to the understanding of sorbitol's electrochemical oxidation by investigating the electrocatalytic behavior of monometallic Au, Pt, and various PtAu alloy nanoparticles. Their research demonstrated that PtAu alloy catalysts not only improved sorbitol oxidation reaction (SOR) efficiency but also promoted the generation of shorter-chain byproducts, attributed to enhanced electron transfer kinetics. Expanding on this, Torres-Pacheco *et al.* [23] researched the electrochemical oxidation of sorbitol in an alkaline environment, using bimetallic catalysts combining palladium and gold (PdxAuy/C). They discovered that while the size and makeup of the catalyst particles were similar, the interactions between the 2 metals (bimetallic interactions) boosted the catalytic activity by changing the catalyst's structure and electron behavior. Among the various catalysts they tested, those with a 60% palladium/40% gold ratio ($Pd_{60}Au_{40}$/C) and a 40% palladium/60% gold ratio ($Pd_{40}Au_{60}$/C) performed the best. In particular, $Pd_{60}Au_{40}$/C generated significantly more current than catalysts made of palladium or gold. This research suggests that these bimetallic palladium-gold catalysts are more active and stable, making them good candidates for future sorbitol fuel cell technologies.

Research on sorbitol membraneless alkaline fuel cells (SMAFCs) remains limited; however, recent studies have begun to explore the electrochemical characteristics of both anodic and cathodic catalysts in alkaline sorbitol solutions. One such investigation successfully synthesized and assessed $AgMn_3O_4$/C, AgSn/C, and Pd/C catalysts for use as both anode and cathode materials in SMAFCs. Through cyclic voltammetry, Pd/C was identified as a highly effective anode catalyst, while $AgMn_3O_4$/C and AgSn/C demonstrated notable resistance to oxidation reactions when employed as cathode catalysts - a critical attribute given the issue of sorbitol crossover from the anode. Nonetheless, the reduction reaction efficiency of these cathode catalysts diminished with increasing sorbitol concentration, indicating interference from fuel crossover. This study advances the understanding of catalyst performance in SMAFCs, highlighting the important role of oxidation resistance in cathode

materials to mitigate the detrimental effects of fuel crossover and optimize cell operation.

Materials and methods

Catalyst synthesis

Catalysts with 20 wt% $AgMn_3O_4$/C and 20 wt% AgSn/C cathodes 20 wt% $AgMn_3O_4$/C

To synthesize silver manganese oxide supported on carbon, 0.63 g of silver nitrate ($AgNO_3$) (Merck) and 0.169 g of potassium manganate ($KMnO_4$) (Merck) were dissolved in 50 mL of deionized water and stirred magnetically for 24 h. The solution's pH was then adjusted to 9 - 11 using 2 M sodium hydroxide (NaOH) (Merck), followed by the addition of 0.40 g sodium borohydride ($NaBH_4$) (Merck). The resulting mixture was further stirred for an additional 24 h. Subsequently, 3.20 g of Vulcan XC–72R carbon (Cabot Company) was introduced, and the suspension was stirred for another 24 h. The resulting precipitate was collected by filtration, washed several times with deionized water, and dried at 80 °C for 24 h to yield the silver manganese oxide/carbon composite.

20 wt% AgSn/C

Initially, 0.63 g of silver nitrate ($AgNO_3$) (Merck) and 0.64 g of tin chloride ($SnCl_2$) (Merck) were dissolved in 50 mL of deionized water and stirred magnetically for 24 h. The pH of the solution was then adjusted to 9 - 11 using 2 M sodium hydroxide (NaOH) (Merck). Subsequently, 0.53 g of sodium borohydride ($NaBH_4$) (Merck) was added, and the mixture was stirred for an additional 24 h. Following this, 3.20 g of Vulcan XC-72R carbon (Cabot Company) was introduced, and the suspension was stirred for another 24 h. The resulting precipitate was collected by filtration, washed repeatedly with deionized water, and dried at 80 °C for 24 h to yield the silver-tin/carbon composite.

Catalyst of the anode with 20 wt% Pd/C

20 wt% Pd/C

A total of 1.33 g of palladium chloride ($PdCl_2$) (Merck) was dissolved in 50 mL of deionized water and stirred magnetically for 24 h. The solution's pH was then adjusted to 9 - 11 using 2 M sodium hydroxide (NaOH) (Merck). Next, 0.4 g of sodium borohydride ($NaBH_4$) (Merck) was added, and the mixture was stirred for an additional 24 h. Afterward, 3.2 g of Vulcan XC-72R carbon (Cabot Company) was introduced, and the suspension was stirred for a further 24 hours. The resulting precipitate was collected by filtration, thoroughly washed with deionized water, and dried at 80 °C for 24 h to yield the palladium-on-carbon catalyst.

Catalyst lnk

A solution of 0.009 g of catalyst was prepared in 5 mL by weighing 0.009 g of catalyst. Then, 3.50 mL of isopropanol solution (Merck) and 1.50 mL of DI water were added to the mixture, after which the substances were dissolved via ultrasonication.

Preparation of the working electrode

Preparing the working electrode involves wiping the glassy carbon surface with ethanol 1-2 times. Once the ethanol solution had completely evaporated, a 1.5 µL drop of Nafion solution (Merck) was applied and the mixture was left for 3 min. Next, 5 µL of the catalyst solution was added and the mixture was allowed to sit for 24 h. to obtain the working electrode containing the catalyst.

Electrochemical characterization of the catalyst

The electrochemical properties of the electrocatalyst samples were examined via cyclic voltammetry (CV). The parameters were configured to include a voltage range from –1.2 V to 1.2 V, with a scan rate of 100 mV/s and a fine scan rate of 10 mV/s.

Nomenclature

n is the number of electrons transfer in the reduction of oxygen

F is Faraday's constant (96,485 mol^{-1})

A is the geometric surface area of RDE (A = 0.196 cm^2)

D is the diffusion coefficient of the oxygen ($cm^2. s^{-1}$)

ν is the kinematic viscosity of the working electrolyte ($cm^2. s^{-1}$)

C_O is oxidant concentration (concentration of oxygen) ($mol.cm^{-3}$)

ω is the angular rotation rate of the electrode (1,600 rpm = 12.946 rad s^{-1})

j_d is limiting current density

j_k is kinetic current density

Results and discussion

This study investigated the electrochemical properties of sorbitol as a fuel for both the cathode (positive electrode) and anode (negative electrode) in alkaline fuel cells, utilizing silver manganese oxide, silver tin, and palladium supported on carbon as electrocatalysts. The research also examined the physical characteristics and catalytic potential of silver manganese oxide, silver tin, and palladium-based electrocatalysts on carbon supports. The research was structured in 2 main parts: 1st, the physical characterization of the silver manganese oxide, silver tin, and palladium electrocatalysts was conducted using scanning electron microscopy (SEM) and elemental analysis; 2nd, the electrochemical performance of these electrocatalysts in facilitating the oxidation of sorbitol fuel in alkaline potassium hydroxide (KOH) solution was evaluated using cyclic voltammetry.

Physical characterization of the catalyst

The 1st part of this research focused on analyzing the physical characteristics of 3 types of electrocatalysts, silver manganese oxide, silver tin, and palladium, supported on carbon substrates. This characterization was carried out using scanning electron microscopy (SEM) in conjunction with scanning transmission electron microscopy (STEM) and energy-dispersive X-ray spectroscopy (EDX) to investigate the morphology and elemental composition of the catalysts.

STEM Techniques.

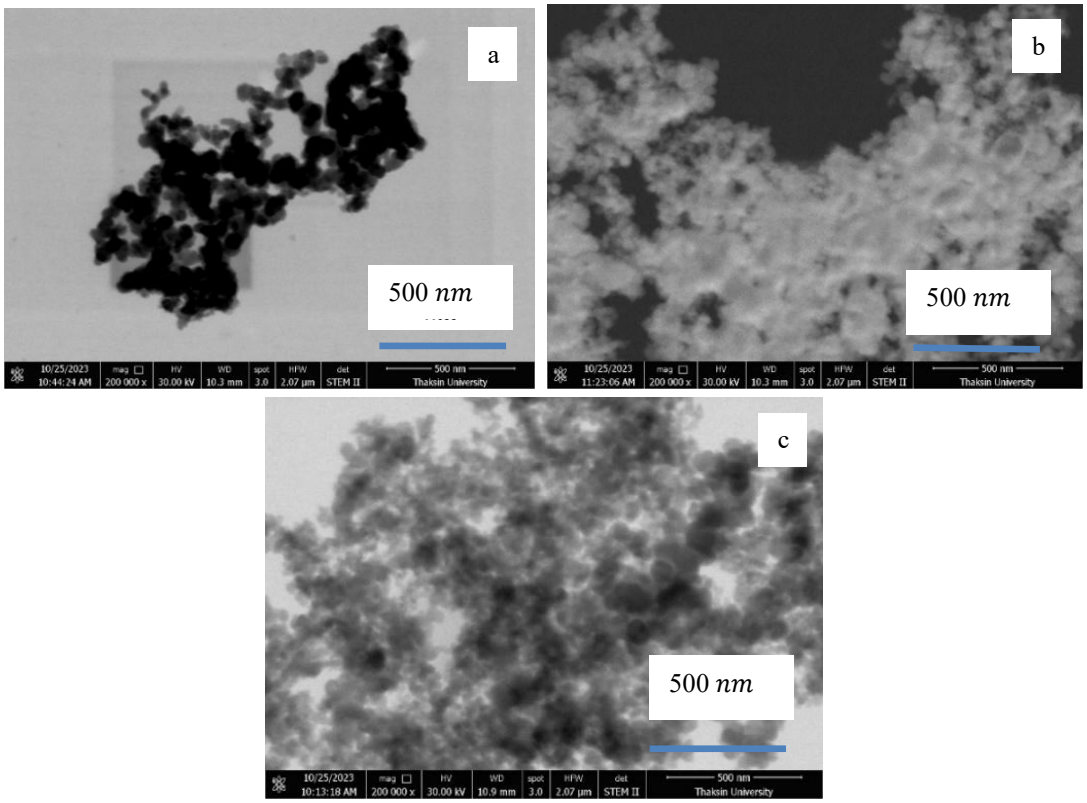

Figure 1 STEM image showing the surface of the $AgMn_3O_4$/C catalyst (a), AgSn/C catalyst (b) and Pd/C catalyst (c).

The $AgMn_3O_4$/C (**Figure 1(a)**) and AgSn/C (**Figure 1(b)**) catalysts are very lumpy and densely clustered on a carbon surface containing small particles.

The Pd/C (**Figure 1(c)**) catalysts are very small, lumpy, and densely clustered on a carbon surface containing small particles.

Table 1 Results of elemental quantification analysis by EDX and XRF for the $AgMn_3O_4$/C, AgSn/C, and Pd/C electrocatalysts.

Catalyst		$AgMn_3O_4$/C		AgSn/C		Pd/C	
Analysis techniques		Mass Concentration (wt %)					
		EDX	XRF	EDX	XRF	EDX	XRF
Type of elemental analysis	Pd	-	-	-	-	4.57	17.50
	Ag	0.07	2.85	2.41	10.01	-	-
	Mn	0.38	18.67	-	-	-	-
	Sn	-	-	1.37	9.09	-	-
	O	12.92	-	6.89	-	7.74	-
	C	86.63	76.73	89.33	75.06	87.7	79.48

Note: Energy element analysis (EDX) and elemental quantity analysis were performed via X-ray fluorescence (XRF).

The catalyst was physically characterized via EDX and XRF. As shown in **Table 1**, the EDS technique measures the percentage of specific elements to study the measurable elemental composition, which may also depend on the distribution of the catalyst particles on the carbon surface. These conditions may cause the measured element percentages to be lower than those calculated during catalyst preparation.

EDX Technique

By utilizing the EDX technique, it is possible to determine the composition of a catalyst at specific locations on its surface. Measuring various elements can produce different values, contingent upon the catalyst's distribution on the carbon surface.

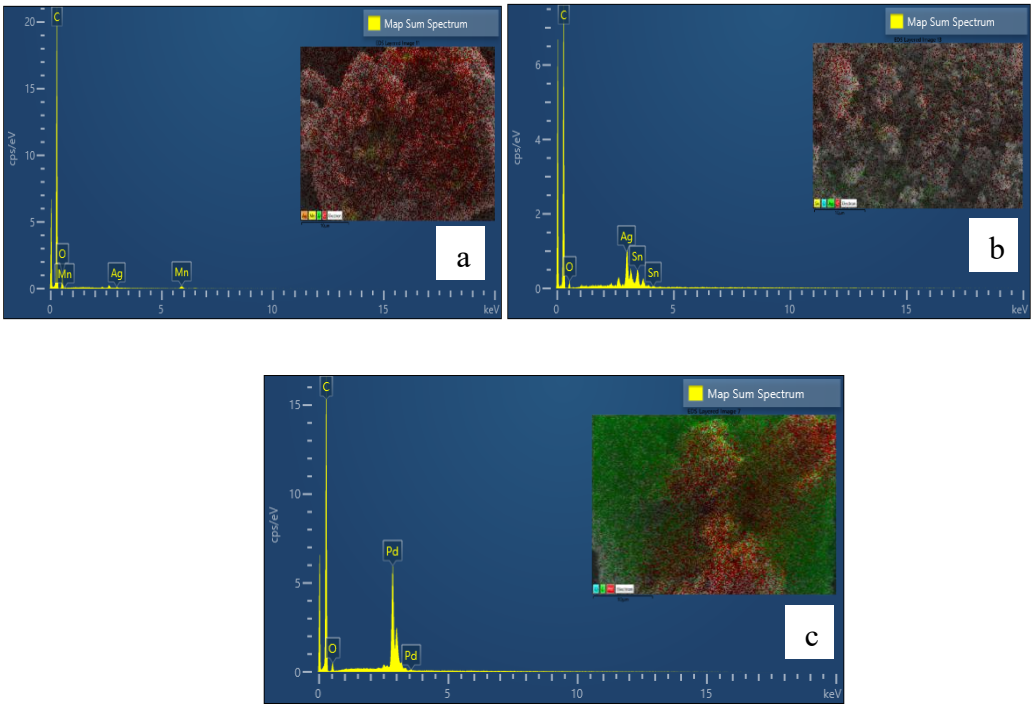

Figure 2 The elemental composition and EDS maps of $AgMn_3O_4$/C (a), the elemental composition of AgSn/C (b), and the elemental composition of Pd/C (c).

EDX was used to measure the $AgMn_3O_4/C$ catalyst (**Figure 2(a)**). The elemental composition was 86.63 wt% C, 0.07 wt% Ag, and 0.38 wt% Mn. EDX was used to measure the AgSn/C catalyst (**Figure 2(b)**). The elemental composition was C (89.33 wt%), Ag (1.37 wt%), and Sn (2.41 wt%). The Pd/C catalyst (**Figure 2(c)**) was subjected to EDX, and the elemental composition of C was 87.7 wt%, whereas that of Pd was 4.57 wt%.

XRD technique

XRD was used to study the physical characteristics of other forms of catalysts. The figure shows the locations of the electrocatalyst peaks on the Vulcan carbon support (XC-72R) and indicates the crystal structures of the metals in different forms. The type of compounds present in the sample clearly shows the peaks of the sample in various planes.

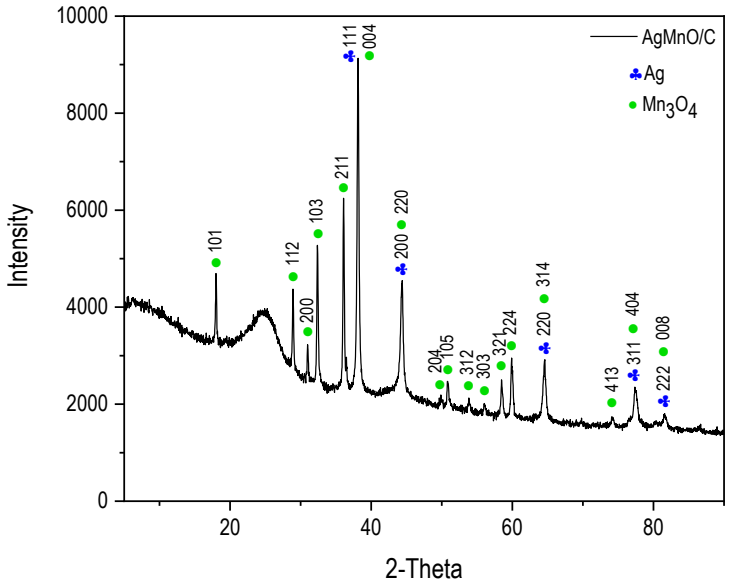

Figure 3 X-ray diffraction pattern of the $AgMn_3O_4/C$ catalyst.

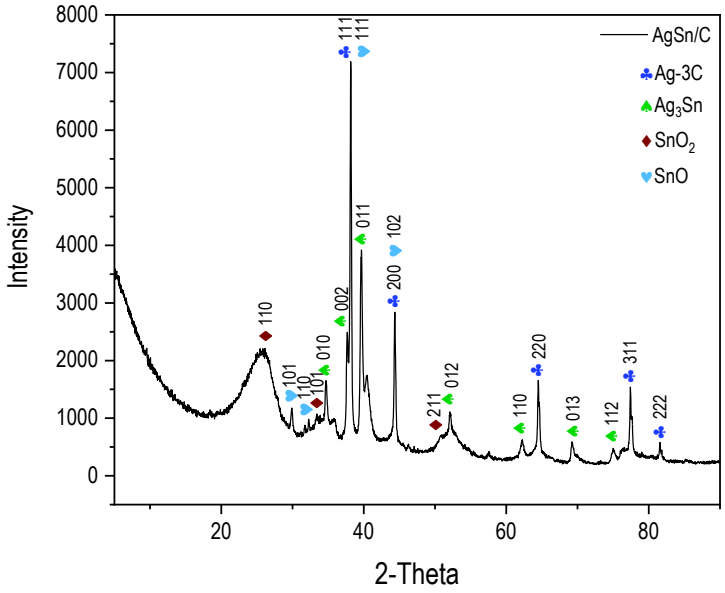

Figure 4 X-ray diffraction pattern of the AgSn/C catalyst.

Figure 3 presents the X-ray diffraction (XRD) patterns of the $AgMn_3O_4$/C and AgSn/C catalysts. Both catalysts exhibit distinct Ag-3C metal peaks at 2θ values of 38.121°, 44.307°, 64.455°, 77.413° and 81.557°, which correspond to the (111), (200), (220), (311), and (222) crystallographic planes (JCPDS 04-0783), confirming the presence of pure cubic-phase silver [24, 25]. Additionally, the $AgMn_3O_4$/C catalyst displays characteristic peaks attributable to Mn_3O_4 particles at 2θ positions of 18.014°, 28.915°, 30.999°, 32.382°, 36.084°, 38.092°, 44.410°, 49.895°, 50.838°, 53.865°, 58.500°, 59.909°, 64.615°, 74.146°, 77.543°, and 81.485°, corresponding to the (101), (112), (200), (103), (211), (004), (220), (204), (105), (312), (321), (224), (314), (413), (404), and (008) planes, respectively (ICDD: 080-0382) [26, 27]. The low intensity and broad width of these Mn_3O_4 peaks indicate both a small quantity and a low degree of crystallinity in the prepared Mn_3O_4 particles. Furthermore, the progressively decreasing intensity of the Mn_3O_4 peaks in the XRD spectra suggests a limited amount of Mn_3O_4 present within the catalyst structure.

Figure 4 illustrates the X-ray diffraction pattern of the AgSn/C catalyst, which exhibits distinct peaks corresponding to Ag_3Sn, SnO_2, and SnO at 2θ values of 34.667°, 37.591°, 39.515°, 52.035°, 62.107°, 69.144°, 74.934°, 26.591°, and 33.888°, as well as at 29.876°, 33.308°, 38.282°, and 44.372°. These peaks are indexed to the (010), (002), (011), (012), (110), (013), and (112) planes of Ag_3Sn, which indicate a hexagonal structure [28]. The observed peaks at 26.591° and 33.888° correspond to the (101) plane of SnO_2 (JCPDS 21-1250), representing the tetragonal rutile phase [29], while peaks at 29.876°, 33.308°, 38.282°, and 44.372° are attributed to the (101), (110), (111), and (102) planes of SnO, consistent with the R-SnO polycrystalline phase (JCPDS 06-0395) [30]. Both $AgMn_3O_4$/C and AgSn/C catalysts display unique metal peaks, with the MnO signature at 38.092° (004) (ICDD: 080-0382) located close to the Ag metal peak at 38.121° (111), suggesting a pronounced presence of the (111) plane and providing a distinguishing feature [31]. The existence of MnO in the cathode catalyst is further corroborated by metal content analysis using EDS, EDS mapping, and XRF, which confirmed the presence and quantification of MnO in the $AgMn_3O_4$/C and AgSn/C catalysts.

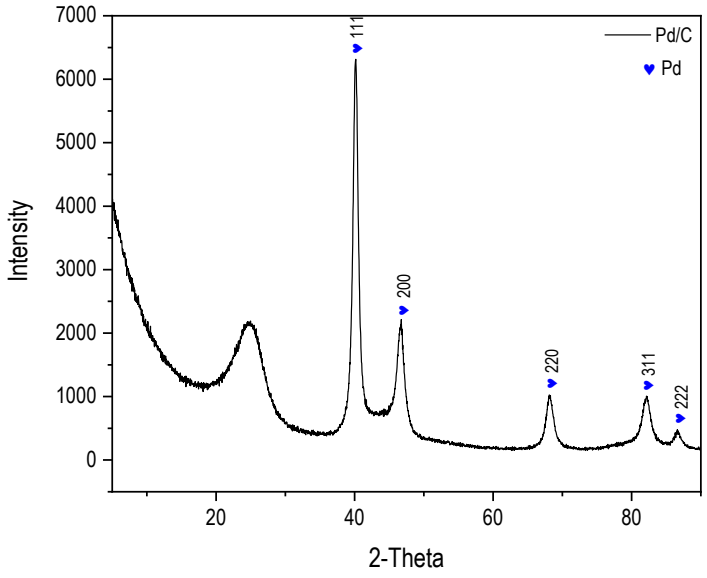

Figure 5 X-ray diffraction pattern of the Pd/C catalyst.

Figure 5 displays the X-ray diffraction (XRD) pattern of the Pd/C catalyst, which exhibits distinct Pd metal peaks at 2θ values of 40.119°, 46.664°, 68.128°, 82.111°, and 86.628°, corresponding to the (111), (200), (220), (311), and (222) crystallographic planes, respectively (JCPDS 87-0641). These results confirm that the palladium in the catalyst adopts a face-centered cubic (fcc) structure [32]. Moreover, the PdBi/C catalyst

presents unique peaks attributable to $Bi_2(CO_3)O_2$ at 2θ values of 12.937°, 23.923°, 26.043°, 30.294°, 32.755°, 40.378°, 42.315°, 46.982°, 52.439° and 56.937°, corresponding to the (002), (101), (004), (103), (110), (105), (114), (200), (107), and (123) planes, respectively (JCPDS 41-1488). These peaks indicate a tetragonal structure consistent with the bismuthite phase, in agreement with the findings of Julio Castillo-Rodríguez [33].

The XRD analysis offers important details about the crystalline structure, phase composition, and particle size of the synthesized AgSn/C, $AgMn_3O_4$/C, and Pd/C catalysts, directly influencing their electrochemical behavior. For instance, the diffraction peaks observed in the Pd/C sample correspond to face-centered cubic (fcc) Pd, indicating a high degree of crystallinity. This structural order facilitates efficient electron transport and enhances catalytic activity, especially in reactions like formic acid oxidation or oxygen reduction [34].

In the case of AgSn/C, XRD patterns may reveal alloy formation or phase segregation between Ag and Sn. The presence of Ag–Sn alloy phases typically improves electrocatalytic properties due to electronic modification of Ag by Sn, which can optimize the adsorption energies of reaction intermediates. Moreover, Sn can enhance CO tolerance and suppress poisoning effects, making AgSn/C a promising catalyst in fuel cell applications [35].

For $AgMn_3O_4$/C, the XRD analysis confirms the presence of spinel Mn_3O_4, which provides multiple redox states (Mn^{2+}/Mn^{3+}) that contribute to superior electrocatalytic activity, particularly for oxygen reduction or oxygen evolution reactions. The combination of Ag and Mn_3O_4 may lead to synergistic effects where Ag enhances conductivity and Mn_3O_4 contributes to redox activity. The relatively broad peaks associated with Mn_3O_4 also suggest nanoscale crystallites, which offer a higher surface area and more active sites for electrochemical reactions [35, 36].

Overall, the structural features revealed by XRD, such as phase purity, alloying effects, and crystallite size, play a fundamental role in determining the catalytic behavior of the materials. The optimized crystalline structure and metal-support interactions improve reaction kinetics, stability, and electrochemical performance.

Electrochemical characterization of the electrocatalysts

The 2nd part of this research investigated the electrochemical behavior of sorbitol fuel at concentrations ranging from 0.1 to 0.5 M in 0.1 M KOH solution, focusing on the impact of 3 types of electrocatalysts - silver manganese oxide, silver tin, and palladium - supported on carbon substrates. Using cyclic voltammetry, this study examined how each catalyst influences the oxidation processes and overall electrochemical performance of sorbitol fuel cells under alkaline conditions

Catalyst for cathode electrodes (Cathodic)

The performance of $AgMn_3O_4$/C catalysts was evaluated in 0.1 M KOH solution across sorbitol concentrations from 0.1 to 0.5 M (**Figure 6**). The introduction of sorbitol influenced the reduction reactions, particularly when $AgMn_3O_4$/C was used as a cathode catalyst. Comparative analyses were also conducted between $AgMn_3O_4$/C and AgSn/C catalysts in the absence of fuel. The $AgMn_3O_4$/C catalyst demonstrated distinct electrochemical behavior at several potential regions: at position 1 (0.10 to –0.06 V), a reduction reaction corresponding to the electron acceptance by MnO occurred (Eq. (1)); at position 2 (–0.08 to –0.27 V), electron absorption by $MnOOHO^-$ was observed (Eq. (2)); and at position 3 (–0.29 to –1.20 V), the regeneration of MnO_2 completed the catalytic cycle (Eq. (3)). These results indicate the importance of cathode-side catalysts possessing both oxidation resistance and the ability to promote reduction reactions. Although the reduction reaction decreased with increasing sorbitol concentrations (0.1 to 0.5 M), the $AgMn_3O_4$/C catalyst maintained notable resistance to oxidation, highlighting its potential suitability for cathodic applications in sorbitol-fueled alkaline fuel cells [37].

$$2MnO_2 + 2H_2O + 2e^- \rightarrow 2MnOOH + 2OH^- \quad (1)$$

$$2MnOOH + O_2 \rightarrow 2(MnOOHO^-) \quad (2)$$

$$2(MnOOHO^-) + 2e^- \rightarrow 2MnO_2 + 2OH^- \quad (3)$$

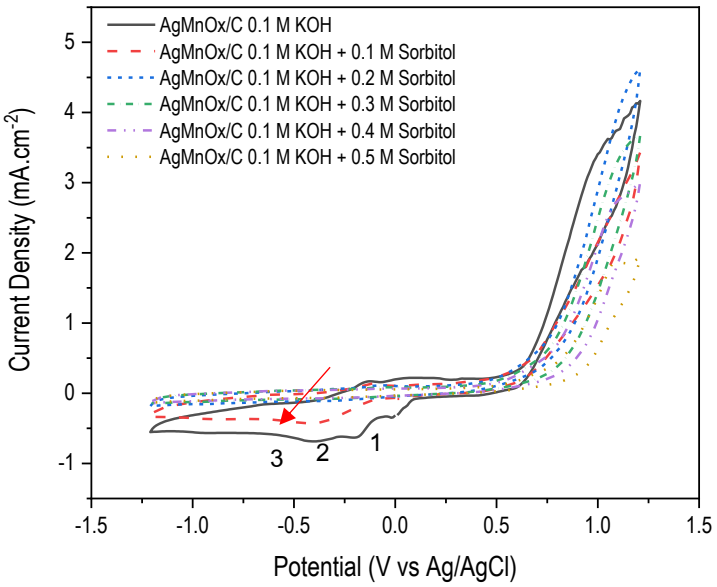

Figure 6 Cyclic voltammogram of the $AgMn_3O_4$/C catalyst in 0.1 M KOH solution doped with 0.1 to 0.5 M sorbitol at a scan rate of 0.01 V/s.

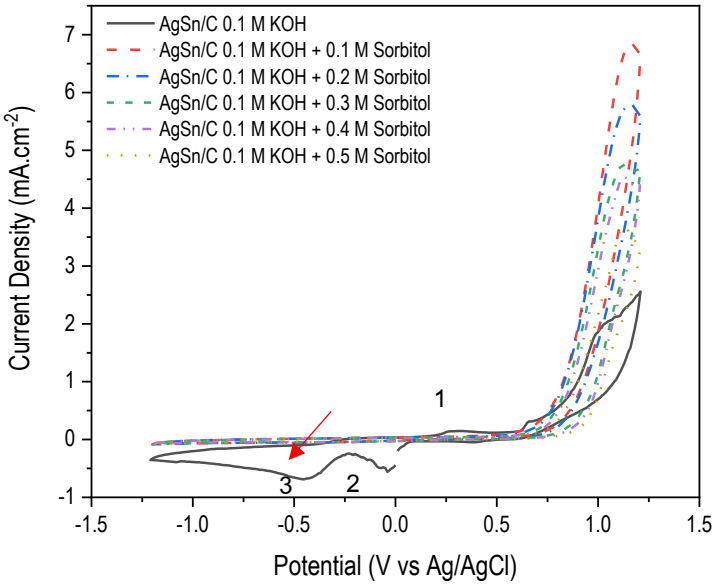

Figure 7 Cyclic voltammogram of the AgSn/C catalyst in 0.1 M KOH solution doped with 0.1 to 0.5 M sorbitol at a scan rate of 0.01 V/s.

The performance of the AgSn/C catalysts was evaluated in a solution of 0.1 M KOH, which had varying concentrations of sorbitol ranging from 0.1 to 0.5 M (**Figure 7**). The AgSn/C catalysts demonstrated cathode-side catalytic properties while exhibiting notable resistance to oxidation at the cathode. However, when doped with the sorbitol solution, the reduction reaction decreased. The electric potential values of the AgSn/C catalysts were analyzed at 3 different positions to assess their performance. In the 1st position, in the absence of mixed fuel, the electric potential ranged from 0.61 to 0.68 V, leading to the formation of AgOH. In the 2nd position, the electric potential ranged from 0.00 to –0.20 V, indicating a reduction reaction involving AgO^- electrons. Finally, in the 3rd position, the electric potential ranged from –0.30 to –1.20 V, representing the catalyst's AgO recovery to facilitate the continuation of the reaction in subsequent scan cycles [38]. Hence, cathode-side catalysts necessitate reduction reactions while maintaining resistance to oxidation at the cathode.

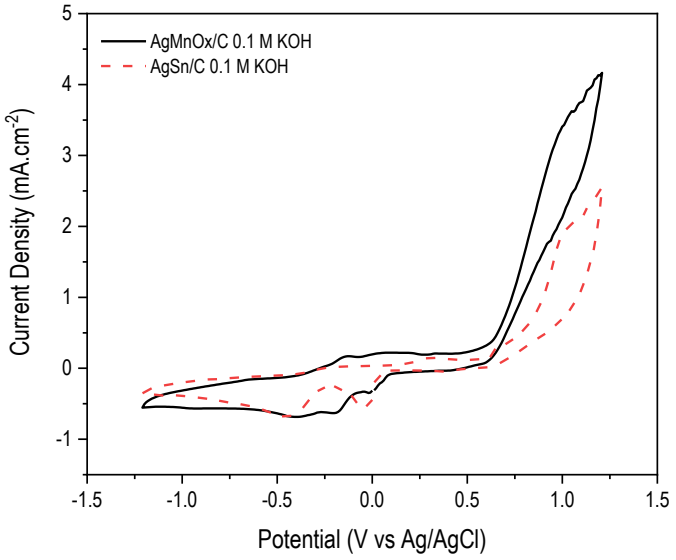

Figure 8 Cyclic voltammograms of the $AgMn_3O_4$/C and AgSn/C catalysts in 0.1 M KOH solution at a scan rate of 0.01 V/s.

Figure 8 presents a comparative analysis of the electrochemical performance of $AgMn_3O_4$/C and AgSn/C catalysts in 0.1 M KOH solution without fuel. The AgSn/C catalyst demonstrated superior reduction activity, operating across a potential range of 0.10 to –1.20 V and achieving a peak reduction current of –0.76 mA·cm^{-2} at –0.50 V. In contrast, the $AgMn_3O_4$/C catalyst also operated within the same potential range, exhibiting a maximum reduction current of –0.68 mA·cm^{-2} at –0.40 V. These results highlight the greater reduction efficiency of the AgSn/C catalyst under these conditions. For optimal cathodic function, catalysts must not only facilitate reduction reactions but also maintain resistance to oxidation, ensuring stability and sustained electrochemical activity at the cathode.

Anode catalyst

The Pd/C catalyst in a 0.1 M KOH solution doped with sorbitol at a 0.1 - 0.5 M concentration was tested at a scan rate of 0.01 V/s (**Figure 9**). The addition of sorbitol to the Pd/C catalyst impacted the oxidation reaction. The Pd/C catalyst is an anode-side catalyst. When Pd/C catalysts are not doped with sorbitol solution, they undergo 3 reduction steps. These positions include the reduction of PdO (as shown in Eq. (4)) and occur in potential ranges of 0.01 to –0.15 V, –0.27 to –0.56, and –0.67 to -1.20 V, respectively. The reduction reaction occurs at positions 1, 2, and 3, resulting in a maximum current density of –1.81 mA.cm^{-2} at a potential of –0.42 V at position 4. Sorbitol exhibited its strongest oxidation reaction at an electric potential of -0.59 V, achieving a current density of 0.50 mA·cm^{-2}. A sorbitol solution was added to the mixture at a 0.1-0.5 M concentration. In that case, an oxidation reaction occurs in the electric potential range of –0.33 to –0.20 V. This reaction can produce a maximum current density of 0.75 mA.cm^{-2} at an electric potential of -0.10 V. Additionally, when a 0.1 M sorbitol solution is added, 2 oxidation positions similar to those in the library, positions 5 and 6, are formed. These positions can be identified through forward scans at potential ranges between –0.67 and –0.34 V and between –0.33 and 0.20 V. The adsorption of sorbitol on the metal (as indicated in Eq. (5)) leads to an oxidation process. At position 7, when a 0.2 - 0.5 M sorbitol solution is mixed, reoxidation occurs due to the reduction of PdO (as shown in Eq. (4)) [38]. As a result, the catalyst on the anode side needs to undergo oxidation. When sorbitol is added as a diluent, the reduction activity decreases and remains steady between 0.1 and 0.5 M.

$$Pd - O + H_2O + 2e^- \rightleftharpoons Pd + 2OH^- \quad (4)$$

$$Pd - (C_6H_{14}O_6) \rightleftharpoons Pd - (C_6H_{14}O_6) \quad (5)$$

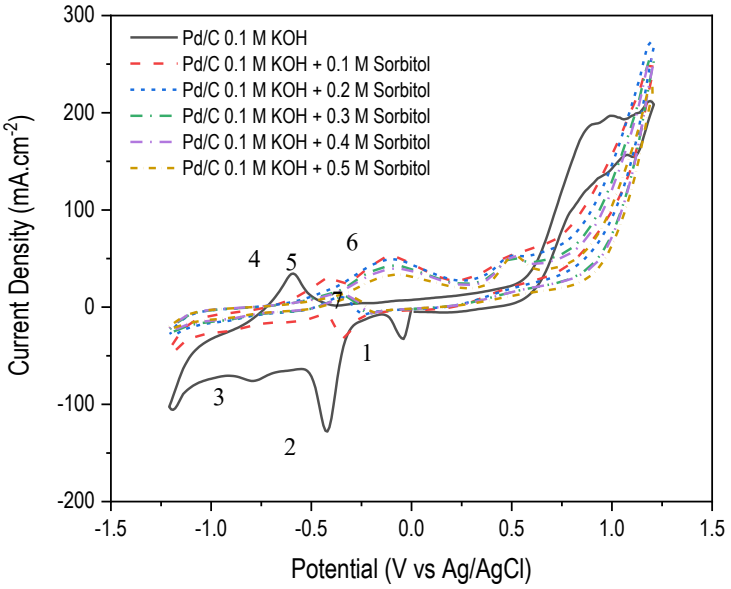

Figure 9 Cyclic voltammograms of the Pd/C catalyst in 0.1 M KOH solution doped with 0.1 to 0.5 M sorbitol at a scan rate. of 0.01 V/s.

The electric potential ranges from 0.60 to 1.20 V (**Figures 6**, **7**, and **9**), and the oxygen evolution reaction (OER) is a limiting reaction in the process of generating molecular oxygen through chemical reaction-electrocatalytic oxygen evolution from oxides. Eqs. (6) to (9) outline the oxygen evolution reaction (OER), which is generally considered to be a 4-step mechanism. Each step in this process involves the transfer of a single electron and proton, with '*' representing an active site on the surface where the reaction intermediates adsorb and react [39].

$$H_2O(l)+^* \rightleftharpoons HO^*+H^+ +e^- \quad (6)$$

$$HO^* \rightleftharpoons O^*+H^+ +e^- \quad (7)$$

$$O^*+H_2O(l) \rightleftharpoons HOO^*+H^+ +e^- \quad (8)$$

$$HOO^* \rightleftharpoons {}^*+O_2(g) + H^+ +e^- \quad (9)$$

An OER volcano curve (potential ranges from 0.60 to 1.20 V), which uses the difference in binding energy between O and OH intermediates as a descriptor, reveals a significant deviation from the ideal oxygen-evolving catalyst's predicted activity (expected at 1.23 eV). This discrepancy arises from scaling relations, which demonstrate an interdependence between the binding energies of OH and OOH intermediates. Consequently, improving OER activity through precise control of intermediate binding energies via synthesis is limited. The primary goal in OER catalyst design is to enhance activity while simultaneously reducing costs [39].

Rotating disk electrode (RDE) technique

The process of studying electrochemical characteristics and operating conditions via a specific technique involves analyzing the catalyst activity data, which can provide insight into various factors, such as the limiting current density of diffusion (DLCD), kinetic limiting current density (KLCD), and number of electrons involved in the catalyst reaction (electron transfer). In this particular study, promising catalysts were selected on the basis of their previous performance in cyclic voltammetry tests. These catalysts, including $AgMn_3O_4$/C and AgSn/C, were further tested in an alkaline potassium hydroxide (KOH) solution with a concentration of 0.1 molar and a sorbitol solution with a concentration of 0.1 molar. The tests were conducted at a scanning rate of 0.01 volts/min, rotating the electrode at different speeds ranging from 400 to 1,800 rpm. The tests were conducted under specific conditions to create a solution saturated with oxygen gas (O_2). **Figures 10(a)** and **10(c)** visually represent the test results obtained from the catalysts via this technique. The measured electric current can be used to calculate various values

via the equation Koutecky-Levich. When a graph showing the relationship between 1/j and $\omega^{(-1/2)}$ is drawn (as in the Equation shown in **Figures 10(b)** and **10(d)**), the slope of the graph line is equal to

$$\frac{1}{0.620nFAD^{2/3}v^{-1/6}C_O}$$

where n is the number of electrons transfer in the reduction of oxygen, F is Faraday's constant (96,485 mol^{-1}), A is the geometric surface area of RDE (A = 0.196 cm^2), D is the diffusion coefficient of the oxygen, ν is the kinematic viscosity of the working electrolyte, C_O is oxidant concentration (concentration of oxygen) and ω is the angular rotation rate of the electrode (1600 rpm = 12.946 rad s^{-1}) [40-42]. The Y-axis intersection is equal to $1/j_k$ [43]. The equation above enables the calculation of the distribution's limiting current density (j_d), kinetic current density (j_k), and number of electrons involved in the catalytic reaction (n). The resulting value of n indicates the calculated value.

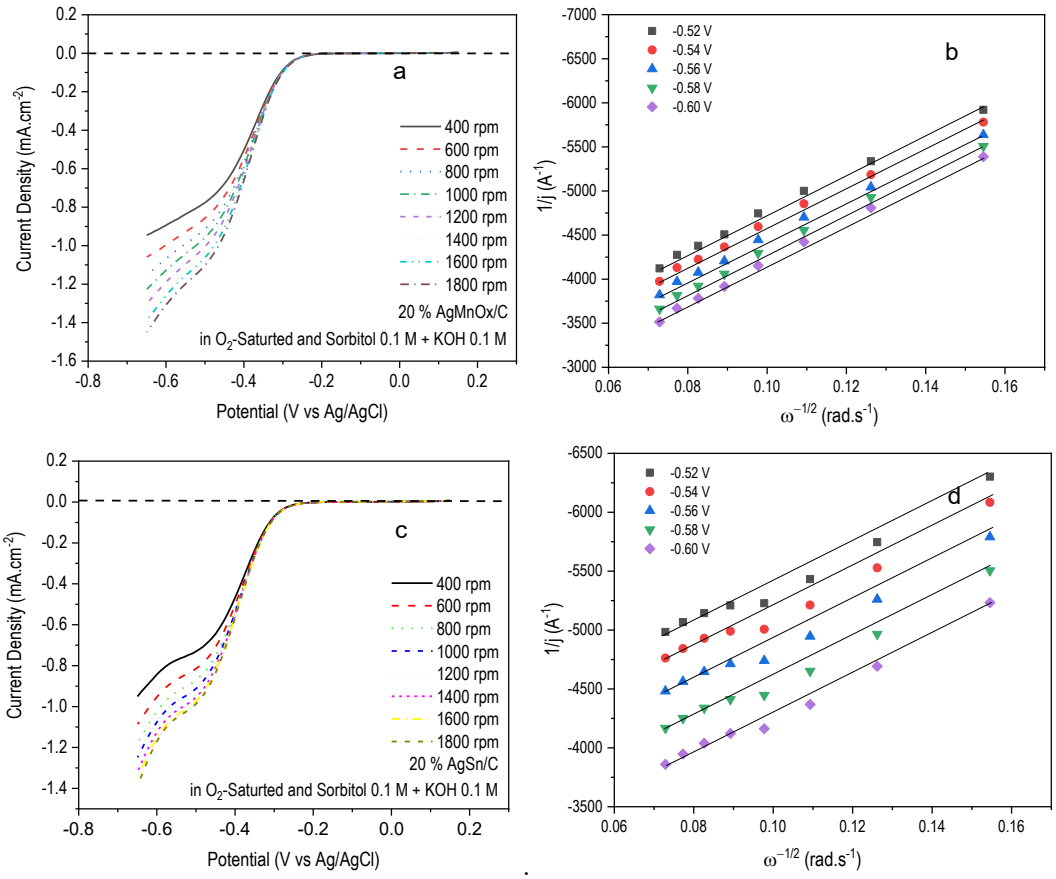

Figure 10 Voltammograms of the $AgMn_3O_4$/C and AgSn/C catalysts (a and c) Linear-sweep voltammograms for the reduction reaction on the catalyst. Controlled rotation of the electrodes at speeds of 400 to 1,800 rpm. (b and d) Koutecky-Levich graph. An alkaline potassium hydroxide (KOH) solution with a concentration of 0.1 M and a sugar solution of sorbitol with a concentration of 0.1 M were used under the condition of oxygen gas (O_2) at a scanning rate of 0.01 V/s.

Figure 10 shows the kinetic parameters that can be used to assess the effectiveness of catalyzing the ORR. These parameters pertain to the electrochemical reaction of the catalyst on the rotating disk electrode. According to Levich's equation, the electric current of the electrodes within a system is influenced by the angular velocity, which is proportional to $\omega^{(1/2)}$. However, when the experiment was conducted at a relatively high angular velocity, the curve deviated from a linear relationship, indicating that the reaction kinetics restricted electron transfer. A lower kinetic current density (j_k) for a catalyst suggests a reduced electron transfer rate in the system. The number of electrons involved in the catalyst's reaction (n) was determined.

As illustrated in **Figure 10(a)**, the $AgMn_3O_4$/C catalyst had an average value of 2.27, which was lower than the average calculated value of 3.20 for the AgSn/C catalyst [38].

Performance of a direct sorbitol fuel cell using an electric potential difference measurement technique

The performance of the sorbitol fuel cells was analyzed by testing a single fuel cell made of transparent acrylic sheet material with a fuel cell design that directly feeds liquid fuel. The fuel cell structure consists of 2 main parts: the cathode side housing and the anode side housing. Carbon cloth on a stainless steel metal plate with a catalyst area of 2.0×2.5 cm and a reaction sample of 50 mg was used as the cathode and anode electrode. An electrode barrier and an air feed plate (air cathode) were used, and the materials used were chromatography paper and carbon cloth coated with PTFE, respectively. The test measured the electrical potential difference via a digital multimeter and the resistance value via decade resistor boxes. The resistance was set to an initial value of 50,000 Ohms and gradually decreased to 0 Ohms by reducing it to 3,000 Ohms. Sorbitol (0.1 M) in 0.1 M potassium hydroxide solution was injected as the fuel solution type into the anode side housing at a flow rate of 0.5 mL/min, while the air was fed into the cathode side housing at a flow rate of 3 mL/min.

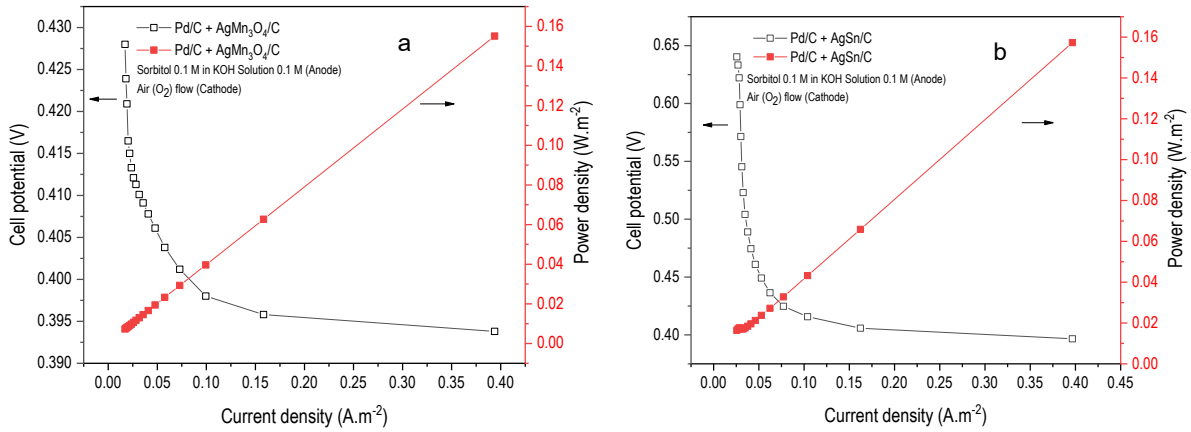

Figure 11 Polarization and power density curves of a sorbitol 0.1M solution with the electrolyte KOH 0.1M, direct-fed alkaline membraneless fuel cell using (a) Pd/C and $AgMn_3O_4$ catalyst electrodes, (b) Pd/C with AgSn/C catalyst electrodes.

Figure 11 shows the polarization and power density of an alkaline membraneless fuel cell directly fueled with sorbitol. Two experiments were conducted: (**Figure 11(a)**) employing Pd/C as the anode and $AgMn_3O_4$/C as the cathode, and (**Figure 11(b)**) using Pd/C as the anode and AgSn/C as the cathode. The experimental series involving Pd/C as the anode and AgSn/C as the cathode yielded the highest current density value of 0.40 $A.m^{-2}$ and the highest power density value of 0.155 $W.m^{-2}$ compared with the experimental results obtained using the Pd/C catalyst as the anode and $AgMn_3O_4$/C as the cathode.

Conclusions

The electrochemical analysis via cyclic voltammetry was carried out by adding the $AgMn_3O_4$/C, AgSn/C, and Pd/C catalysts in a 0.1 M KOH solution containing sorbitol ranging from 0.1 to 0.5 M. The scan rate was maintained at 0.01 V/s for both the cathode and anode sections. The addition of sorbitol, at concentrations ranging from 0.1 to 0.5 M to a 0.1 M KOH solution of $AgMn_3O_4$/C and AgSn/C catalysts during dilution at a scan rate of 0.01 V/s had an impact on the reduction reaction. The catalyst must resist cathode oxidation to function effectively since the cathode side requires a reduction reaction. In the context of the sorbitol membraneless fuel cell discussed previously, both $AgMn_3O_4$/C and AgSn/C represent promising non-platinum group metal alternatives for the cathode. The choice between them would depend on specific performance targets (e.g., peak power density, long-term stability, tolerance to specific fuel

components) and the ease/cost of scalable synthesis for the desired performance.

However, the reduction reaction decreased when the concentration of sorbitol increased. To ensure an effective and appropriate electric cell for the anode oxidation peak of the Pd/C catalyst, it is necessary to select a stable and long-lasting catalyst that can withstand oxidation. The selection of such a catalyst will allow for the highest potential difference in the potential range of –0.5 to 0.5 V, resulting in oxidation sites. The oxidation peak of the Pd/C catalyst at the highest current density was 0.75 $mA.cm^{-2}$ in a 0.1 M KOH solution diluted with 0.1 M sorbitol. The Pd/C catalyst exhibited a good oxidation reaction at the anode, which increased with increasing temperature. The hydrodynamic voltammetry technique and controlled rotation disk electrode (RDE) yielded positive results for the AgSn/C catalyst, indicating good kinetics and favorable working conditions. The catalyst was tested in a solution saturated with oxygen gas (O_2) at a scan rate of 0.01 V/s, and the average calculated value of the number of electrons involved in the catalytic reaction (n) was determined to be 3.20. The electric potential difference measurement technique was also used to evaluate a single cell of a sorbitol membraneless alkaline fuel cell (SMAFC). The fuel substance used was a sorbitol fuel solution (0.1 M) fed into the anode side with potassium hydroxide solution (0.1 M). The anode was supplied with a 2.5 mL/min flow rate, while the air was fed into the cathode housing at a 3 mL/min flow rate. The experiments revealed that the highest current density value of 0.40 $A.m^{-2}$ and the highest power density of 0.155 $W.m^{-2}$ were obtained from a series of experiments conducted between the Pd/C catalyst (anode terminal) and AgSn/C (cathode terminal).

This research significantly advances our understanding of catalyst performance in sorbitol membraneless alkaline fuel cells (SMAFC), particularly emphasizing why a cathode's oxidation resistance is crucial due to fuel (sorbitol) crossover. This sentence highlights that cutting-edge research in catalysts goes beyond finding a material that works. It involves sophisticated material synthesis and engineering at the atomic and nanoscale levels to create catalysts with specific defects and microstructures that are precisely tuned to maximize the efficiency of the electrochemical reactions in alkaline fuel cells.

Acknowledgments

This research was supported by Thailand Science Research and Innovation (TSRI), Thailand-funded 2022.

Declaration of generative AI in scientific writing

The authors acknowledge the use of generative AI tools (e.g., Grammarly and ChatGPT by OpenAI) in the preparation of this manuscript, specifically for language editing and grammar correction. No content generation or data interpretation was performed by AI. The authors take full responsibility for the content and conclusions of this work.

CRediT Author Statement

Pintira Chayboonchoo: Data curation, Formal analysis, Investigation, Validation, Visualization, and Writing – original draft.

Supansa Dampat: Data curation, Formal analysis, Investigation, Validation, and Visualization**.**

Sonchai Intachai: Data curation, Formal analysis, Investigation, Validation, and Visualization**.**

Bancha Yingngam: Data curation, Formal analysis, Investigation, Validation, and Visualization**.**

Chakkrapong Chaiburi: Methodology, Project administration, Resources, Supervision, Validation, Funding acquisition, and Writing **–** original draft**.**

References

[1] A Harjanne and JM Korhonenc. Abandoning the concept of renewable energy. *Energy Policy* 2019; **127**, 330-340.

[2] T Seetawan. Alternative energy: Future energy. *Journal of Industrial Technology and Innovation* 2022; **1(1)**, 1.

[3] W Palasai and P Phrommes. A case studying of light source used in combination of small-sized regenerative fuel cell system. *Princess of Naradhiwas University Journal* 2017; **9(1)**, 86-99.

[4] O Muneeb, E Do, D Boyd, J Perez and JL Haan. PdCu/C anode catalysts for the alkaline ascorbate fuel cell. *Applied Energy* 2019; **235**, 473-479.

[5] S Lekapat and S Teekasap. Fuel cell. *EAU Heritage Journal Science and Technology* 2013; **7(1)**, 1-10.

[6] E Gülzow. Alkaline fuel cells. *Fuel Cells* 2004; **4(4)**, 251-255.

[7] F Bidault and PH Middleton. *Alkaline fuel cells: Theory and application. In:* TM Letcher (Ed.). *Comprehensive Renewable Energy* 2012; **4**, 179-202.

[8] LJ Torres-Pacheco, L Álvarez-Contreras, V Lair, M Cassir, J Ledesma-García, M Guerra-Balcázar and N Arjona. Electrocatalytic evaluation of sorbitol oxidation as a promising fuel in energy conversion using Au/C, Pd/C and Au–Pd/C synthesized through ionic liquids. *Fuel* 2019; **250**, 103-116.

[9] I Kruusenberg, L Matisen, Q Shah, AM Kannan and K Tammeveski. Non-platinum cathode catalysts for alkaline membrane fuel cells. *International Journal of Hydrogen Energy* 2012; **37(5)**, 4406-4412.

[10] J Weiss, H Zhang and P Zelenay. Recent progress in the durability of Fe-N-C oxygen reduction electrocatalysts for polymer electrolyte fuel cells. *Journal of Electroanalytical Chemistry* 2020; **875(15)**, 114696.

[11] W Xu, R Zeng, M Rebarchik, A Posada-Borbon, H Li, CJ Pollock, M Mavrikakis and HD Abruna. Atomically dispersed Zn/Co-N-C as ORR electrocatalysts for alkaline fuel cells. *Journal of the American Chemical Society* 2024; **146(4)**, 2593-2603.

[12] JH Ho, Y Li, Y Dai, T Kim, J Wang, J Ren, HS Yun and X Liu. Ionothermal synthesis of N-doped carbon supported $CoMn_2O_4$ nanoparticles as ORR catalyst in direct glucose alkaline fuel cell. *International Journal of Hydrogen Energy* 2021; **46(39)**, 20503-20515.

[13] J Hu, H Lu, M Li, G Xiao, M Li, X Xiang, Z Lu and Y Qiao. Cobalt valence modulating in CoOx incorporated carbon nanofiber for enhanced glucose electrooxidation. *Materials Reports: Energy* 2022; **2(2)**, 100091.

[14] Y Dai, J Ding, J Li, Y Li, Y Zong, P Zhang, Z Wang and X Liu. N, S and transition-metal co-doped graphene nanocomposites as high-performance catalyst for glucose oxidation in a direct glucose alkaline fuel cell. *Nanomaterials* 2021; **11(1)**, 202.

[15] T Suzuki, M Fujino, and Y Yamada. Formation of a palladium catalyst layer using an anionic Surfactant and subsequent fabrication of a glucose fuel cell. *Journal of Chemical Education* 2023; **100(12)**, 4780-4785.

[16] J Huang, P Simons, Y Sunada, J Rupp and S Yagi. Pt-catalyzed d-glucose oxidation reactions for glucose fuel cells. *Journal of The Electrochemical Society* 2021; **168**, 064511.

[17] X Xu, X Dong, D Li, M Qi and H Huang. ZIF-8-derived three-dimensional nitrogen-doped porous carbon as a Pt catalyst support for electrocatalytic oxidation of glucose in a glucose fuel cell. *ACS Applied Energy Materials* 2023; **6(5)**, 2886-2896.

[18] D Basu and S Basu. A study on direct glucose and fructose alkaline fuel cell. *Electrochimica Acta* 2010; **55(20)**, 5775-5779.

[19] T Liu. Glucose fuel cells and membranes: A brief overview and literature analysis. *Sustainability* 2022; **14(14)**, 8376.

[20] Z Daşdelen, A Özcan and A Özcan. Preparation of anode catalysts for sorbitol electrooxidation based on the nanocomposites of fumed silica, reduced graphene oxide and gold nanoparticles. *International Journal of Hydrogen Energy* 2021; **46(55)**, 28121-28133.

[21] MB Askari, P Salarizadeh and AD Bartolomeo. $NiCo_2O_4$-rGO/Pt as a robust nanocatalyst for sorbitol electrooxidation. *International Journal of Energy Research* 2022; **46(5)**, 6745-6754.

[22] LJ Torres-Pacheco, AD Leon-Rodriguez, L Álvarez-Contreras, M Guerra-Balcazar and N Arjona. Sorbitol electro-oxidation reaction on sub < 10 nm PtAu bimetallic nanoparticles. *Electrochimica Acta* 2020; **353**, 136593.

[23] LJ Torres-Pacheco, AD Leon-Rodriguez, JA Bañuelos, L Álvarez-Contreras, M Guerra-Balcázar and N Arjona. Electrocatalytic oxidation of sorbitol on PdxAuy/C bimetallic nanocatalysts. *Fuel* 2022; **314**, 122788.

[24] C Liu, X Yang, H Yuan, Z Zhou and D Xiao. Preparation of silver nanoparticle and its application to the determination of ct-DNA. *Sensors* 2007; **7(5)**, 708-718.

[25] DVKD Sara, A Rouhollahi, SM Pourmortazavi and M Shamsipur. High current density chronopotentiometric electrosynthesis and SEM

characterization of hexanethiol-monolayer-protected silver planar nanotriangles (Ag@C6SH). *Journal of Nanomaterials* 2016; **1**, 1-12.

[26] R Tholkappiyan, AN Naveen, K Vishista and F Hamed. Investigation on the electrochemical performance of hausmannite Mn_3O_4 nanoparticles by ultrasonic irradiation assisted co-precipitation method for supercapacitor electrodes. *Journal of Taibah University for Science* 2018; **12(5)**, 669-677.

[27] BGS Raj, AM Asiri, JJ Wu and S Anandan. Synthesis of Mn_3O_4 nanoparticles via chemical precipitation approach for supercapacitor application. *Journal of Alloys and Compounds* 2015; **636(7)**, 234-240.

[28] SZ Kure-Chu and H Yashiro. Corrosion resistance of multilayered Sn/Ag_3Sn films electroplated on Cu alloys for highly reliable automotive connectors. *Journal of The Electrochemical Society* 2014; **161(10)**, C441-C449.

[29] W Chen, Q Zhou, F Wan and T Gao. Gas sensing properties and mechanism of nano-SnO2-based sensor for hydrogen and carbon monoxide. *Journal of Nanomaterials* 2012; **2012(20)**, 1-9.

[30] LY Liang, ZM Liu, HT Cao and XQ Pan. Microstructural, optical, and electrical properties of SnO thin films prepared on quartz via a two-step method. *ACS Applied Materials & Interfaces* 2010; **2(4)**, 1060-1065.

[31] F Akbar, M Tariq, HU Khan, J Khan, MK Uddin, SS Ahmed and A Rahim. Development of Ag-Ni NPs loaded on MWCNTs for highly sensitive, selective and reproducible nonenzymatic electrochemical detection of glucose. *Journal of Materials Science: Materials in Electronics* 2021; **32(12)**, 16166-16181.

[32] M Khan, M Khan, M Kuniyil, SF Adil, A Al-Warthan, HZ Alkhathlan, W Tremel, MN Tahir and MRH Siddiqui. Biogenic synthesis of palladium nanoparticles using *Pulicaria glutinosa* extract and their catalytic activity towards the Suzuki coupling reaction. *Dalton Transactions* 2014; **43(24)**, 9026-9031.

[33] J Castillo-Rodríguez, C Tzompantzi-Flores, Y Piña-Pérez, F Tzompantzi, P Salinas-Hernández, F Morales-Anzures, CE Santolalla-Vargas and R Gómez. High photoactivity of $Bi_2O_2(CO_3)/Zn_5(CO_3)_2(OH)_6$ prepared by a facile one-pot synthesis for the efficient degradation of phenol under UV light. *Journal of Photochemistry and Photobiology A: Chemistry* 2020; **402(CO3)**, 112816.

[34] S Yu,Q Han,Y Yang, X Ma, L Gao, S Yan, Y Wu and L Lu. Electrochemical performance of the Pd/C catalyst synthesized by polyol process. *International Journal of Electrochemical Science* 2019; **14(8)**, 7871-7883.

[35] K Iwase, T Kamimura and I Honma. Ag-Sn intermetallic compounds synthesized via mechanical alloying as electrocatalysts for CO_2 reduction reaction. *Electrochemistry* 2024; **92(7)**, 077001.

[36] IG Kim, F Ghani, KY Lee, S Park, S Kwak, HS Kim, IW Nah and JC Lim. Electrochemical performance of Mn_3O_4 nanorods by N-doped reduced graphene oxide using ultrasonic spray pyrolysis for lithium storage. *International Journal of Energy Research* 2020; **44(6)**, 1-14.

[37] MA Kostowskyj, DW Kirk and SJ Thorpe. Ag and Ag–Mn nanowire catalysts for alkaline fuel cells. *International Journal of Energy Research* 2010; **35(11)**, 5666-5672.

[38] C Chakkrapong, S Kantrakorn and B Sitanan. Efficiency of cathode catalyst between Ag/C and AgMnxOy/C for glucose membraneless alkaline fuel cell. *Journal of Applied Research on Science and Technology* 2022, **21(2)**, 126-136.

[39] R Pittkowski, P Krtil and J Rossmeis. Rationality in the new oxygen evolution catalyst development. *Current Opinion in Electrochemistry* 2018; **12**, 218-224.

[40] G Koscher and K Kordesh. Can refillable alkaline methanol-air systems replace metal-air cells? *Journal of Power Sources* 2004; **136(2)**, 215-219.

[41] J Qiao, L Xu, L Ding, P Shi, R Baker and J Zhang. Effect of KOH concentration on the oxygen reduction kinetics catalyzed by heat-treated Co-Pyridine/C electrocatalysts. *International Journal of Electrochemical Science* 2013; **8(1)**, 1189-1208.

[42] M Chatenet, MB Molina-Concha, N El-Kissi, G Parrour and JP Diard. Direct rotating ring-disk measurement of the sodium borohydride diffusion coefficient in sodium hydroxide solutions. *Electrochimica Acta* 2009; **54(18)**, 4426-4435.

[43] M Hunsom. *PEM fuel cell and electrochemical analysis.* Chulalongkorn University Press, Bankok, 2012.